applied sciences

MDPI

Article

Constrained Dynamic Optimization of the Sit-to-Stand Task

Amur AlYahmedi [1,*], Sarra Gismelseed [2] and Riadh Zaier [1]

[1] Department of Mechanical & Industrial Engineering, College of Engineering, Sultan Qaboos University, Muscat 123, Oman; zaier@squ.edu.om
[2] Department of System Engineering, Military Technological College, Muscat 111, Oman; saraabbasher91@gmail.com
* Correspondence: amery@squ.edu.om; Tel.: +968-95209194

Featured Application

One potential application of this work is in the design and optimization of assistive technologies such as lower-limb exoskeletons and rehabilitation devices. By predicting how joint torques, trunk motion, and ground reaction forces change with seat height, movement speed, and reduced joint strength, the proposed model can help define actuator requirements and adaptive control strategies for individuals with impaired mobility. Furthermore, it may support clinical rehabilitation by providing a framework to assess task difficulty and optimize environmental conditions, such as seat height, to enhance safety and functional independence.

Abstract

This study develops a reduced-order predictive model of the Sit-To-Stand (STS) task to examine whether a simplified biomechanical representation can reproduce key STS patterns reported in the literature and to investigate the role played in movement by a flexible trunk. The model represents the human body as a planar multibody system and formulates STS as an optimization problem within a discrete mechanics framework. This formulation combines reduced model complexity, explicit torso flexibility, and a structure-preserving numerical approach for trajectory generation. Simulations were used to evaluate the effects of movement duration, reduced joint strength, and seat height on joint torques, kinematics, trunk motion, and ground reaction forces (GRFs). The results reproduced several qualitative trends reported in previous experimental studies, including increased peak joint torques and GRFs with shorter movement duration, lower joint strength, and reduced seat height, as well as greater compensatory trunk motion under more demanding conditions. These findings suggest that the proposed framework captures key adaptive features of STS mechanics and may provide useful insights for rehabilitation analysis and the design of assistive technologies such as lower-limb exoskeletons and rehabilitation devices. At the same time, the present work should be regarded as an initial methodological study, since validation is currently qualitative and further experimental calibration, quantitative validation, and sensitivity analysis remain part of ongoing work.

Keywords: Sit-To-Stand (STS); multibody dynamics; optimization

Academic Editor: Arkady Voloshin

Received: 27 February 2026
Revised: 3 April 2026
Accepted: 5 April 2026
Published: 10 April 2026

1. Introduction

Understanding Sit-To-Stand (STS) motion is important in clinical, rehabilitation, and athletic settings because it reflects lower-limb strength, balance, coordination, and neuromuscular control. Patients recovering from stroke often exhibit impaired muscle coordi-

nation that affects their ability to rise from a chair, while older adults with osteoarthritis or sarcopenia may experience difficulty because of reduced joint strength and/or loss of muscle mass [1]. Since STS is performed frequently in daily life, on average about 60 times per day [2], even modest impairments can substantially affect independence and quality of life. More generally, age-related decline and pathological conditions can compromise the ability to perform STS effectively [3–5]. Consequently, STS has become an important functional means of assessing and monitoring mobility. Previous studies have shown, for example, that examining healthy individuals' adaptations to changes such as chair height may help in diagnosing functional limitations [6], that the five-repetition STS test provides a reliable measure of lower-body muscle and joint function [7], and that age influences trunk flexion, lower-extremity muscle activity, and postural stability during STS [8]. A recurring conclusion in this literature is that trunk motion plays a central role in the successful execution of STS. The torso contributes not only to posture but also to momentum generation, whole-body coordination, and the transfer from sitting equilibrium to standing balance. In this context, the authors of [9] highlighted the importance of the torso in mobility and suggested that flexible torso representations may improve the prediction of movement in both healthy and impaired individuals. Similarly, in [10], the authors showed that spinal kinematics differ significantly in patients with low back pain, supporting the need for multi-segmental or flexible trunk analysis when the objective is to better understand functional movement. This broader perspective is important because STS and related tasks such as sit-to-walk are not governed by lower-limb mechanics alone; rather, they emerge from coordinated whole-body motion, including the trunk. Understanding how healthy individuals perform STS and STW may therefore help guide the design, assessment, and improvement of assistive strategies and devices for older adults and for individuals with impairments [11–14].

The biomechanics and determinants of STS have been studied extensively, including the effect of seat height [15–19] and the role trunk-focused exercise combined with physical therapy plays in improving mobility and balance after stroke [20].

In parallel, modelling studies have contributed substantially to the biomechanical understanding of STS [21–24] and to the development of assistive approaches [25–27]. Optimization-based methods have also been used to predict STS motion and investigate movement strategies. For example, in [28], the authors formulated STS prediction as a nonlinear optimization problem, and their results showed qualitative agreement with experimental findings reported in the literature. The authors of [29] employed a multi-phase cost function to generate utility-optimized trajectories for rehabilitation-related applications. Early work by the authors of [30] formulated STS as an optimization problem and argued that gradual muscle force variation better reflects human biomechanics.

The authors of [31] used a skeletal and muscular model to improve STS movement and reduce knee stress through genetic optimization, with subsequent experimental support for the model behaviour. Likewise, in [32], the authors employed a three-dimensional bipedal model to improve torque requirements during STS and compared the resulting predictions with experimental observations, including ground reaction force data.

Despite these important contributions, the literature still leaves an important scientific gap. Existing STS studies have improved understanding of the task, but they do not yet fully provide predictive biomechanical models that are simple enough for systematic analysis and optimization while still sufficiently expressive to examine movement abnormalities, functional limitations, and the potential effects of intervention. More specifically, although the importance of trunk motion is widely recognized, the torso is often represented in a simplified or effectively rigid manner, and the implications of introducing additional torso degrees of freedom are not always examined in a way that clarifies their mechanical

contribution. As a result, how a reduced-order but flexible torso model can be used to study normal STS mechanics, abnormal movement patterns, and the possible effect of rehabilitative or assistive interventions remains unresolved.

A further gap concerns the numerical framework used to formulate and solve the predictive problem. In the present work, the problem of optimal control is formulated within a discrete mechanics framework. Unlike approaches that begin by directly discretizing the differential equations of motion, discrete mechanics starts by discretizing the underlying variational principle itself. This distinction is important because it leads to structure-preserving numerical schemes, commonly referred to as variational integrators, that inherit the characteristic properties of the underlying mechanical system. In particular, these methods are known for preserving symplectic structure, exhibiting favourable long-term energy behaviour with reduced numerical drift and providing a mechanically consistent framework for the simulation and optimization of dynamical systems over extended horizons. Such properties are especially attractive in predictive biomechanical modelling, where the objective is not only to reproduce a movement but also to examine how model structure, assumptions, or parameter changes affect the resulting motion.

Accordingly, the scientific gap addressed in this study is the lack of a predictive STS model that simultaneously combines (i) a flexible representation of the torso, (ii) reduced complexity that supports interpretation and optimization, and (iii) a structure-preserving discrete mechanics formulation suitable for predictive analysis. The central hypothesis of this work is that a simplified biomechanical model with a flexible torso, when posed as an optimization problem within a discrete mechanics framework, can capture the essential dynamics of STS more effectively than rigid reduced-order representations while remaining more interpretable and computationally manageable than highly detailed full-body models. More specifically, we hypothesize that the inclusion of degrees of freedom for the torso within this framework will improve the predictive description of STS motion and provide a useful basis for studying functional limitations, abnormal movement, and the potential effects of rehabilitation or assistive intervention.

According to this aim, the present study develops a flexible-torso STS model that is intentionally simple while still capable of representing key dynamic features of the movement. The problem is posed as an optimization task in a discrete mechanics setting so that relevant determinants of STS performance can be analysed within a numerically robust and mechanically consistent framework. At the same time, the present work should be regarded as an initial step rather than a complete validation study. At this stage, the model has been examined primarily through qualitative comparison with behaviours and trends reported in the literature rather than through direct quantitative experimental validation. In addition, comprehensive sensitivity analysis with respect to parameter variation has not yet been completed, and the parameters used in the model have not yet been calibrated through dedicated experiments. These limitations are acknowledged explicitly, and their resolution forms part of the ongoing work, which will focus on experimental validation, parameter calibration, and quantitative assessment of model sensitivity and predictive performance. In this regard, electromyography (EMG) recordings and force-platform measurements represent natural experimental counterparts for validating and refining the model predictions and are identified as a priority direction for future experimental work.

2. The STS Task Formulated as an Optimization Problem

Since STS transfer is a symmetrical movement primarily occurring in the sagittal plane, it can be simplified as a two-dimensional problem within that plane. This study employs a six-link model representing the shank, thigh, and head–arms–trunk (HAT) segments. The trunk is presumed flexible and approximated as discrete, rigid segments that are

interconnected by flexible joints. These joints are equipped with springs and dampers, which allow for deformation by providing the necessary degrees of freedom (DOFs). The springs and dampers model the body's elasticity and damping characteristics, while the rigid segments simplify the calculation of inertial effects. A schematic showing the model employed in our study is shown in Figure 1.

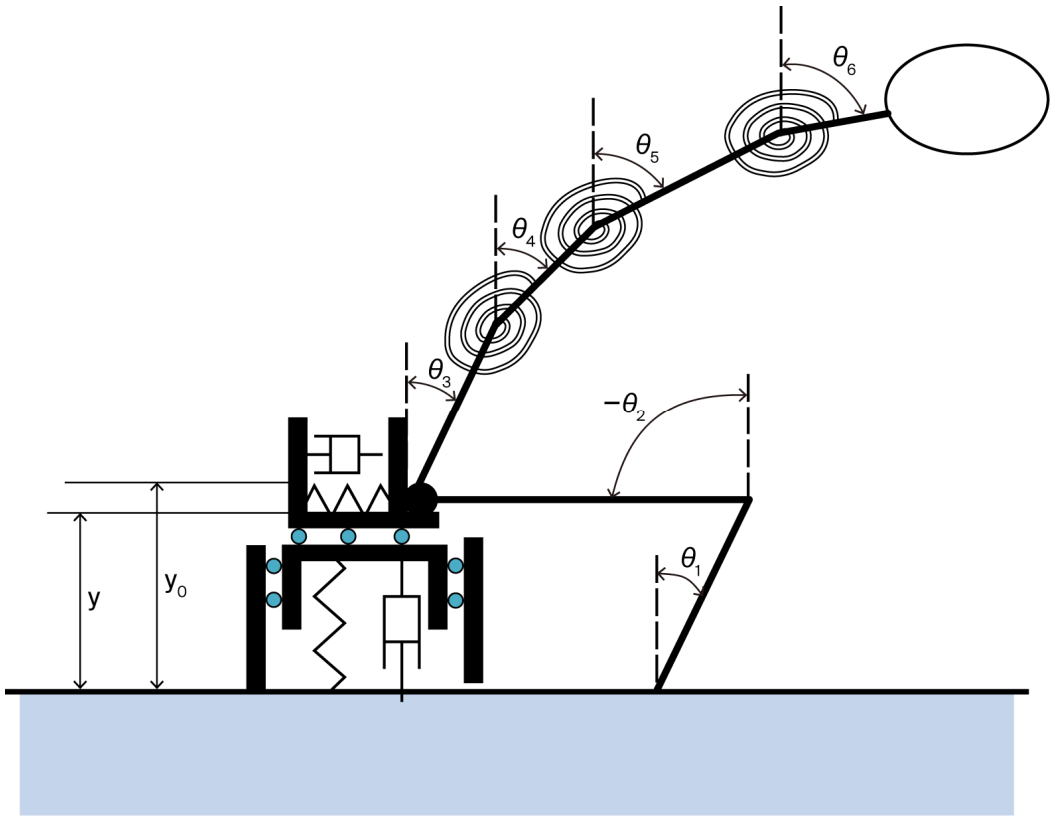

Figure 1. Six-link model (flexible torso).

Discrete mechanics [33] principles are followed in posing the STS as an optimization problem. In contrast to conventional techniques that impose equations of motion as external constraints, discrete mechanics weaves them directly into the optimization process through a discretized form of the Euler–Lagrange equations. This integration preserves the system's underlying geometric structure—safeguarding momentum and, in certain cases, energy—thus enhancing stability, physical realism, and computational efficiency. The outcome is a cohesive and resilient framework, ideally suited to capturing the synchronized, force-driven essence of STS motion. The Lagrange equation is given by

$$\begin{gathered}\mathcal{L} = \frac{1}{2}\dot{v}_{G1}^2\frac{1}{2}I_1\dot{\theta}_1^2 + \ldots + \frac{1}{2}\dot{v}_{G6}^2\frac{1}{2}I_6\dot{\theta}_6^2 \\ -gm_1y_{G1}\ldots - gm_6y_{G6} \\ -\frac{1}{2}k_3(\theta_3-\theta_2) - \frac{1}{2}k_4(\theta_4-\theta_3) - \frac{1}{2}k_5(\theta_5-\theta_4) \\ -\frac{1}{2}k_6(\theta_6-\theta_5)\end{gathered} \tag{1}$$

The Raleigh dissipation function is

$$R = \frac{1}{2}c_3\left(\dot{\theta}_3-\dot{\theta}_2\right)^2 + \frac{1}{2}c_4\left(\dot{\theta}_4-\dot{\theta}_3\right)^2 + \frac{1}{2}c_5\left(\dot{\theta}_5-\dot{\theta}_4\right)^2 + \frac{1}{2}c_6\left(\dot{\theta}_6-\dot{\theta}_5\right)^2$$

Applying the midpoint rule to the continuous Lagrange equation yields the discrete Lagrange equation as follows:

$$\mathcal{L}(q,\dot{q}) \rightarrow h\mathcal{L}_d\left(\frac{q_{k+1}+q_k}{2}, \frac{q_{k+1}-q_k}{h}\right) \tag{2}$$

The system dynamics can be formulated as follows:

$$\begin{gathered} D_1\mathcal{L}_d(\theta_{1k},\theta_{1k+1},\theta_{2k},\theta_{2k+1},\ldots,\theta_{6k},\theta_{6k+1})+ \\ {f_d}^-(\theta_{1k},\theta_{1k+1},\theta_{2k},\theta_{2k+1},\ldots,\theta_{6k},\theta_{6k+1})+ \\ D_2\mathcal{L}_d(\theta_{1k},\theta_{1k+1},\theta_{2k},\theta_{2k+1},\theta_{3k},\ldots,\theta_{6k},\theta_{6k+1})+ \\ {f_d}^+(\theta_{1k},\theta_{1k+1},\theta_{2k},\theta_{2k+1},\ldots,\theta_{6k},\theta_{6k+1}) = 0 \end{gathered} \tag{3}$$

where $D_1L_d(\theta_{1k},\theta_{1k+1},\theta_{2k},\theta_{2k+1},\ldots,\theta_{6k},\theta_{6k+1})$ is the first derivative of discrete Lagrange with respect to current coordinates (i.e., θ_{1k}, θ_{2k}, …, and θ_{6k}), and D_2L_d is the first derivative of discrete Lagrange with respect to future coordinates (i.e., $\theta_{1k+1}, \theta_{2k+1}$, …, and θ_{6k+1}).

$$D_1\mathcal{L}_d = \begin{bmatrix} \frac{\partial\mathcal{L}_d}{\partial\theta_{1k}}(\theta_{1k},\theta_{1k+1},\theta_{2k},\theta_{2k+1},\ldots,\theta_{6k+1}) \\ \cdots \\ \frac{\partial\mathcal{L}_d}{\partial\theta_{6k}}(\theta_{1k},\theta_{1k+1},\theta_{2k},\theta_{2k+1},\ldots,\theta_{6k},\theta_{6k+1}) \end{bmatrix} \tag{4}$$

$$D_2\mathcal{L}_d = \begin{bmatrix} \frac{\partial\mathcal{L}_d}{\partial\theta_{1k+1}}(\theta_{1k},\theta_{1k+1},\theta_{2k},\theta_{2k+1},\ldots,\theta_{6k},\theta_{6k+1}) \\ \cdots \\ \frac{\partial\mathcal{L}_d}{\partial\theta_{6k+1}}(\theta_{1k},\theta_{1k+1},\theta_{2k},\theta_{2k+1},\ldots,\theta_{6k+1}) \end{bmatrix} \tag{5}$$

Both discrete forces, i.e., left and right forces, are defined as the torque applied to each joint.

$${f_d}^- = {f_d}^+ = \begin{bmatrix} u_{1k}-u_{2k} \\ u_{2k}-u_{3k} \\ \vdots \\ u_{6k} \end{bmatrix} \tag{6}$$

An optimal control problem is formulated to replicate the STS task, aiming to minimize a specified cost function. Additional algebraic constraints model the contact between the chair and the segment representing the patient's pelvis, as well as the initial and final positions and velocities of various body segments. Biomechanically appropriate constraints are imposed on joint torques, angular displacements, and angular velocities.

In the results presented here, the cost function is defined as the sum of the squared torques applied to each joint, combined with the sum of the squared time derivatives of those torques.

The initial poster position assumes that the nature of the sitting position for a human being requires that the tibiae (Link 1) have an angle of 0° from the vertical, whereas the femurs (Link 2) have an angle that depends on the seat height. The torso (Links 3, 4, 5, and 6) has an angle of 0°, as defined in our model. With these initial conditions, the optimal control problem is formulated by minimizing a cost function composed of the squared joint torques and the squared torque rates so as to represent both reduced mechanical effort and smoother actuation profiles.

$$\text{Min } J = \sum_{k=1}^{N}\sum_{i=1}^{6}\alpha_i {u_i}^2(k) + \sum_{k=1}^{N}\sum_{i=1}^{6}{\dot{u}_i}^2(k) \tag{7}$$

with decision variables θ_i and u_i.

In accordance with the dynamical equations of motion (Equation (3)), a given set of initial states (the rotational displacement of links and their angular velocities), a prespecified set of terminal constraints (the rotational displacement of links and their angular velocities), and a set of inequality constraints are imposed on the torques and angular displacements.

$$\begin{aligned} \theta_{i\ min} \leq \theta_i \leq \theta_{i\ max} \\ u_{i\ min} \leq u_i \leq u_{i\ max} \end{aligned} \tag{8}$$

A key distinction between rising from a squatting position and rising from a seated position is the motion constraint imposed by the chair. The method for calculating the horizontal and vertical force components exerted by the chair on the model is detailed below, adapted from [30].

$\Delta\vec{u} = J^T F$, $\Delta\vec{u}$ is the projection of the forces to Joints 1 and 2, and J is the Jacobian and F is the horizontal and vertical component of the force at the hip, as computed in Equation (9).

The model of the seat can be generated with a nonlinear spring and a linear damper, as follows:

$$\begin{aligned} F_x &= \begin{cases} 0.5\left(10^{\alpha|\Delta x|}\right) - \beta\dot{x} & \Delta x \leq 0 \\ -0.5\left(10^{\alpha|\Delta x|}\right) - \beta\dot{x} & \Delta x > 0 \end{cases} \\ F_y &= \begin{cases} 0.5\left(10^{\alpha|\Delta y|}\right) - \beta\dot{y} & \Delta y \leq 0 \\ 0 & \Delta y > 0 \end{cases} \end{aligned} \tag{9}$$

Note that F_x and F_y represent the horizontal and vertical components, respectively, of the reaction force exerted on the model by the chair. The resulting nonlinear programming problem was solved using SNOPT, version 7.5, a large-scale sparse optimizer based on sequential quadratic programming (SQP). In SNOPT, each iteration solves a quadratic programming subproblem constructed from a quadratic approximation of the Lagrangian and a linearization of the constraints. Convergence was checked by repeating the optimization with progressively finer temporal discretization and verifying stabilization of the objective value, state trajectories, and control histories.

3. Optimization Results

The human body comprises a variety of tissues and structures that support and facilitate the movement of the skeletal system. This is particularly evident in the trunk, which incorporates a spine divided into multiple segments to allow for flexibility and complex motion [34,35]. In our model, the trunk is represented as a collection of rigid segments, each characterized by specific mechanical properties such as length, mass, stiffness, and damping. These properties are crucial to accurately simulating human movement.

Numerous studies have highlighted the challenges of precisely determining these parameters due to individual variability, environmental influences, and experimental limitations. As a result, many researchers have focused on optimizing (tunning) these parameters to better mimic the dynamics of human movement. Typically, such studies divide the trunk, including the head and neck, into discrete segments, assigning unique mechanical properties to each. However, not all studies provide a comprehensive set of parameters for every trunk segment.

For example, the authors of [35] employed a finite element model of a seated human body with a total mass of 68.6 kg and a height of 175 cm, as detailed in Table 1.

Table 1. The physical parameters were adopted from [35] as literature-sourced baseline values and mapped to the segment definitions of our reduced-order model; they were used as initial estimates to ensure mechanical consistency but were not yet calibrated to subject-specific experimental data.

Segment	Mass (kg)	Length (m)	Com (m)	Moment of Inertia	Joint Stiffness (N·m/rad)	Joint Damping (N·m·s/rad)
Head and neck	5.41	0.2705	0.078	0.036	1000	50
Upper torso	21.89	0.2749	0.33	0.546	2000	10
Lower torso	4.25	0.1281	0.03	0.022	1500	30
Pelvis	2.57	0.1718	0.02	0.01	-	-
Femur	25.95	0.4198	0.309	0.403	-	-
Legs	7.01	0.4384	0.42	0.113	-	-

We used the parameter values listed in Table 1, which were taken from the literature, and observed qualitative rather than exact quantitative agreement between the model response and the reported behaviour. Figure 2 shows the centre of gravity (COG) trajectory in the sagittal plane as predicted by our model and as reported by the authors of [12]. Figure 3 shows the ground reaction force as compared to the experimental results reported in [36].

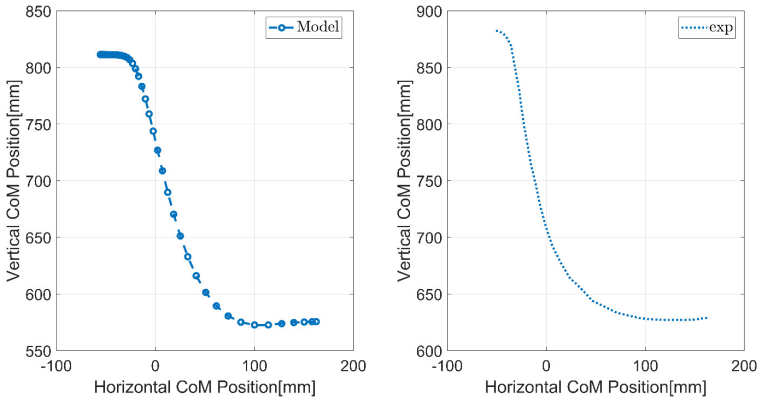

Figure 2. Experimental data (dotted line on the (**right**)) vs. model−produced data (**left**). Experimental data are those reported in [12].

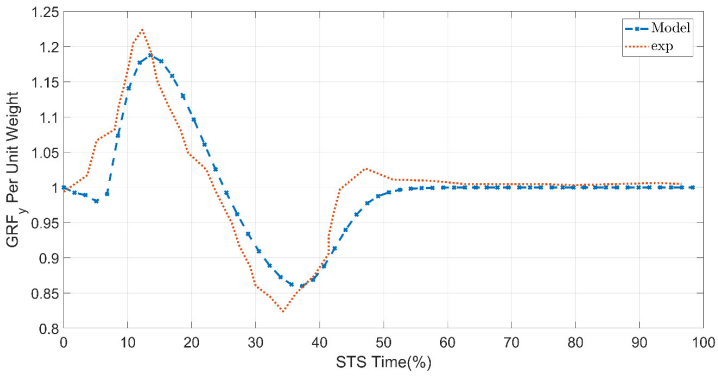

Figure 3. Experimental data sourced from [36].

Referring to the first phase (flexion momentum) in Figure 4, the motion begins with the initiation phase, characterized by forward flexion of the trunk, which generates flexion momentum. This phase ends just before the hip lifts off the surface of the chair. During this time, the centre of gravity (COG) moves forward horizontally with minimal vertical displacement.

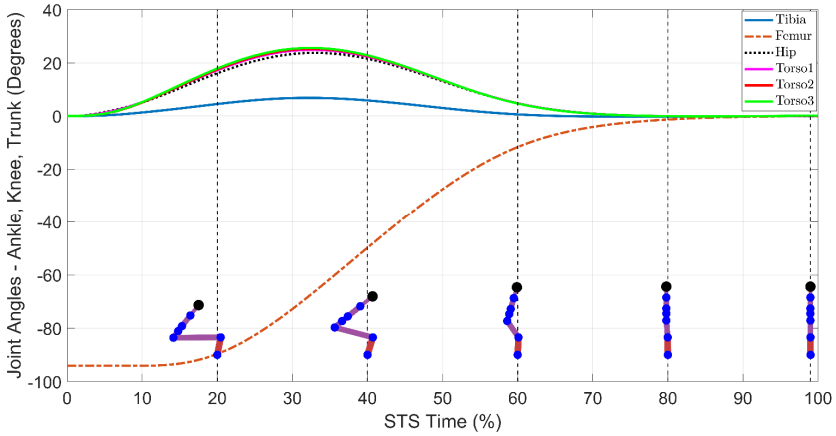

Figure 4. Phases of STS, the black dot represents the head, while the blue dots represent the various joints.

The second phase, known as the momentum transfer phase, starts with the hip lifting off the chair surface (starting at around 18% of the total time of the complete motion). It utilizes the flexion momentum to propel the torso upward and forward, concluding just before the lower leg ceases forward flexion and the ankle reaches maximum dorsiflexion (shortly after 40% of the total time). Throughout this phase, the whole body moves forward and upward. As the hip leaves the chair, body weight shifts onto the feet, placing significant load on the knee joints—making this the most demanding phase for the lower limbs.

The third phase, the extension phase, is marked by the extension of the hips and knees. It begins at maximum ankle dorsiflexion (at 40% of the total time) and ends just before the lower leg stops moving backward (at 80% of the total time).

The final phase, the stabilization phase, starts when the lower leg no longer flexes backward (at 80% of the total time) and is primarily focused on maintaining balance at the terminal standing position.

3.1. STS Speed

To study how STS duration affects the dynamics of the joints of the bipedal model, we aimed to optimize the torques of the joints during standing from a sitting position over different periods: 1.0 s, 1.3 s, 1.8 s, and 2.3 s.

$$J = \sum_{k=1}^{N} \sum_{i=1}^{6} {u_i}^2(k) + \sum_{k=1}^{N} \sum_{i=1}^{6} {\dot{u}_i}^2(k) \tag{10}$$

The observed behaviour of the torques of the tibia, femur, and hip joints can be explained from a biomechanics standpoint. The tibia torque is the effort applied by the tibia muscles, represented by ankle dorsiflexion, to lift the body up and stabilize the ankle during the initial phase of the STS motion; the femur torque is the effort applied by the quadriceps muscle to extend the knee and overcome the inertia to lift the whole body up. The tibia torque demonstrates how the hip extensors contribute to stabilizing the body (especially during the last phase) and propelling it forward. Varying the profile of previously explained torques, as shown in Figure 5, demonstrates how the STS duration affects the magnitude of the joint parameters and the coordination of joint movement. Longer STS durations represent slower and less aggressive movement in terms of the peaks and phases inherent to completing the motion. As shown in Figure 5, increasing the STS duration reduces the peak torque at each joint, which can be explained by the distribution of the load over a longer duration and thereby avoidance of immediate torque from the muscles.

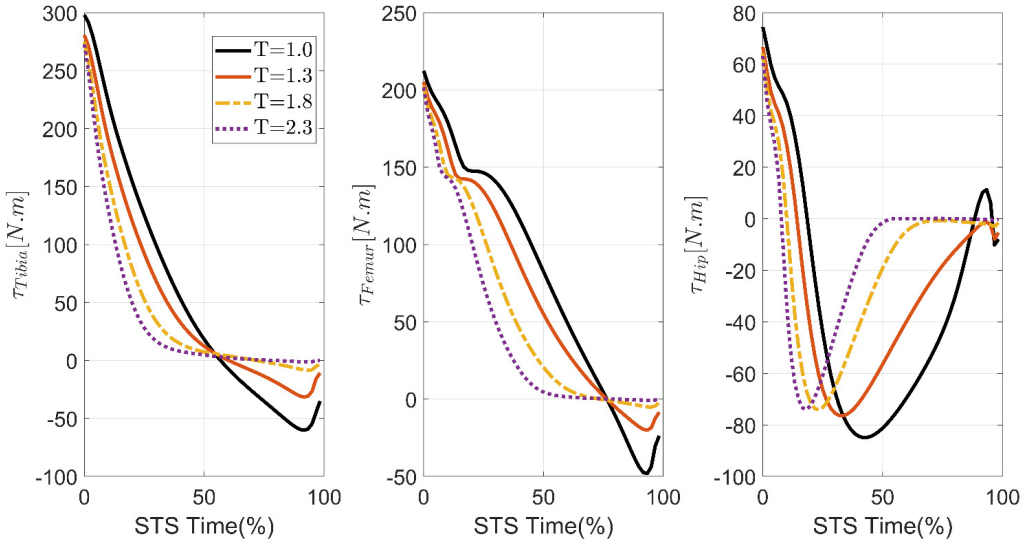

Figure 5. Joint torque (N·m) as STS speed is varied.

The variation also has an obvious effect on the dynamics of joint angles and angular velocities, as seen in Figure 6. Reducing STS duration results in a rapid tilting of the tibia and hip extension to shift the COG forward, which is associated with high angular velocities during the initial phase, whereas the peak at the middle of the angular position and the associated velocity are required to shift the body vertically. Longer STS durations decrease these peaks and result in smother transitions from one phase to another, as is clear from Figure 6 during the transitions between the phases 0–30% of total STS, 30–70% of total STS, and 70–100% of total STS, as well as the longer phases at the end of the STS motion representing body stabilization.

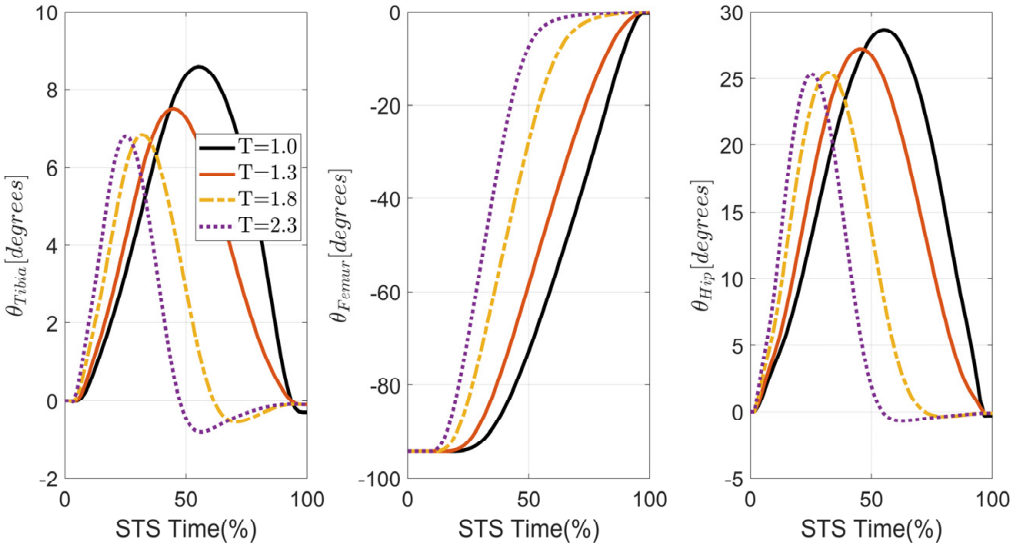

Figure 6. Angular joint position in degrees vs. STS Time (%).

Experimental studies have also explored how the speed of STS movement affects joint kinetics and kinematics. In [37–39], the authors found that reducing the time required to accomplish the STS motion results in an increase in the joint torque, angular motion, and angular velocity due to the muscles producing effort more quickly. It has been shown, in other studies, that increasing the duration of the STS motion produces lower GRF peaks [40,41].

3.2. Weakened Joint Strength

To examine the impact of reduced knee strength, we assigned weighted penalties to joint torque within the optimization, applying a higher weight to the knee joint to simulate diminished torque capacity (Joint 2).

$$J = \sum_{k=1}^{N} \sum_{i=1}^{6} \alpha_i {u_i}^2(k) + \sum_{k=1}^{N} \sum_{i=1}^{6} {\dot{u}_i}^2(k)$$
$$\alpha_i = 1, for\, i = 1,3,4,5,6, \tag{11}$$

The results are as shown in Figures 7 and 8. Restricting knee flexion necessitates higher hip angular velocity to compensate for the loss of range of motion, as seen in Figure 8; this aligns with the results reported in [19]. However, it differs from earlier work [38], in which the authors suggested that peak hip moments may not significantly increase in some patients with limited knee flexion. This divergence highlights the importance of individualized assessments, as compensatory mechanisms may vary based on the degree of restriction and patient-specific factors.

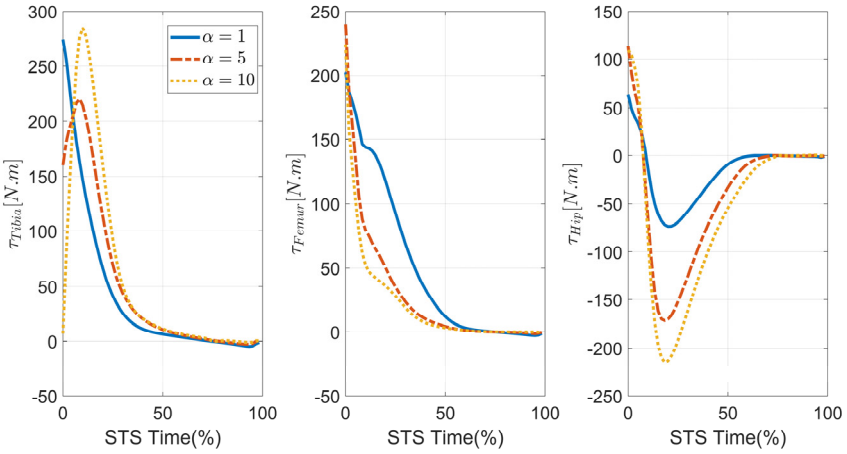

Figure 7. Joint torque in N·m.

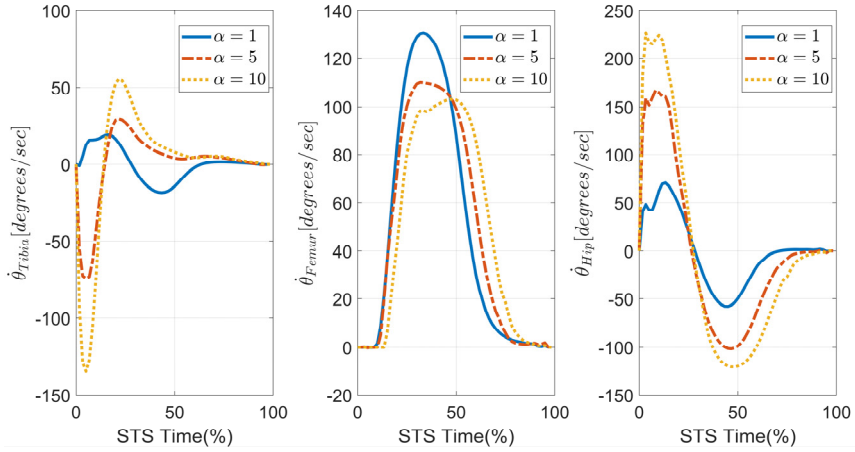

Figure 8. Joint angular velocities in degrees/s.

3.3. Seat Height

Seat height is considered to be one of the main determinants of STS because it can directly influence the success of the motion. We investigated how the body adapts to varying seat heights by formulating an optimization problem that minimizes joint torque

while promoting smooth transitions through the inclusion of torque rate changes in the objective function as follows:

$$J = \sum_{k=1}^{N} \sum_{i=1}^{6} {u_i}^2(k) + \sum_{k=1}^{N} \sum_{i=1}^{6} {\dot{u}_i}^2(k) \quad (12)$$

The results show a consistent pattern for joint angle and joint angular velocity across different seat heights. However, as seen in Figure 9, reducing the seat height results in joints having a larger range of motion, which is apparent because the biped will initially be sitting at more flexed positions, and the hip and knee will require greater extension to transition to the standing position. Meanwhile, the increment in the angle of the tibia indicates that it is positioned with greater flexion due to the reduced seat height [19]. The increment in the range of motion leads to an increase in the joint velocity to attain the fully extended position from more flexed positions over a fixed STS time [19].

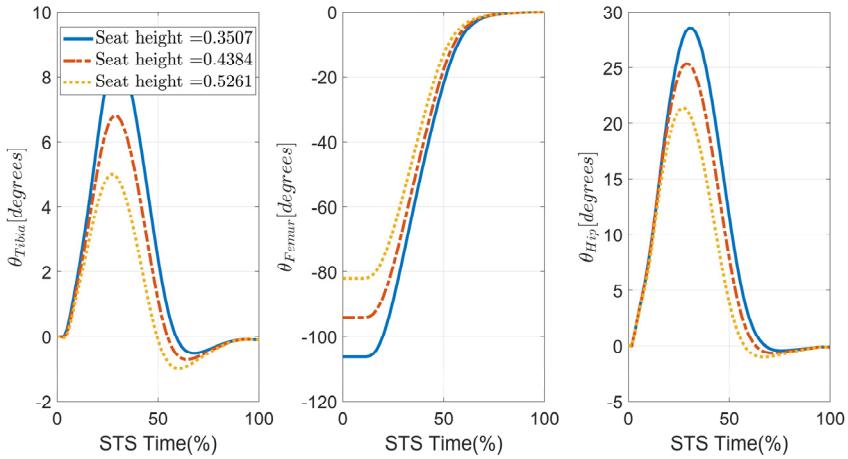

Figure 9. Joint angle in degrees with varying seat height.

On the other hand, the profile of joint torque remains consistent with different seat heights, with small increments on the peak values, especially for hip torque. Lower seat heights require greater torso flexion, which results in a greater mechanical effort to shift the body's centre of gravity toward the base of support during the momentum transfer phase. A small delay in the stabilization phase was noticed as the seat height was decreased.

Due to the increase in effort applied by the muscles to reach the fully extended position from the more flexed position, we noticed an increment in the peak of the GRF. These results confirm results obtained experimentally by the authors of [42], in which it was reported that peak GRF increases due to the higher effort needed to raise the body from a lower seat height.

3.4. Modifying the Initial Trunk Orientation

Beginning with increased trunk flexion results in the duration of the extension phase being lengthened, as seen in Figure 10 (which is obvious since the first phase is no longer needed) [43]. This strategy allows for reduced knee joint moments, making the motion more efficient, as reported in [19]. Another key observation concerns the sequence of joint activation. With active hip flexion, movement initiates at the knee, followed by the hip and ankle. In contrast, without hip flexion, the sequence begins at the hip, then proceeds to the knee and ankle—consistent with the findings in [43]. Contrary to the observation reported by the authors of [43] regarding an active support moment in which the degree of upper-body flexion did not influence the magnitude of the support moment, we found

that the support moment (the sum of individual joint moments) increases when there is no hip flexion.

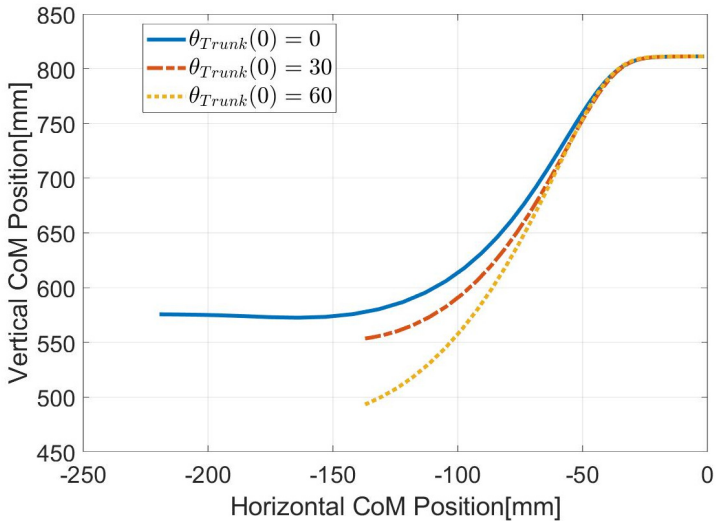

Figure 10. Changing the Initial Position of the Trunk.

4. Discussion and Conclusions

This study presents a reduced-order predictive model of the Sit-To-Stand (STS) task incorporating a flexible torso, formulated within a discrete mechanics-based optimization framework. The primary contribution is methodological: the proposed approach occupies an intermediate position between rigid reduced-order formulations and detailed musculoskeletal models by explicitly accounting for torso flexibility while retaining computational simplicity. This makes it particularly suited for interpretive and parametric analysis rather than subject-specific prediction.

The simulations reproduced several qualitative trends documented in the literature, including increased joint torque and angular velocity with shorter movement durations, increased compensatory trunk motion under reduced knee strength, and greater trunk flexion and ground reaction force at lower seat heights. These results suggest that the framework can capture key adaptive features of STS mechanics within a simplified predictive setting and may offer a useful basis for examining how task conditions and functional limitations modulate mechanical demands.

From an application standpoint, the predicted torque profiles and compensatory motion patterns may provide preliminary insight into mechanically demanding phases of STS, which is relevant to the design of assistive devices and rehabilitation strategies. However, it should be emphasized that the present results are primarily qualitative, as the model has not yet been calibrated against subject-specific data or validated through direct quantitative comparison with experimental measurements. Subject-specific application would therefore require dedicated experimental calibration.

Several limitations bound the current scope of the work. Quantitative experimental validation against motion-capture and force-platform data has not yet been conducted, and a systematic sensitivity analysis of model parameters remains to be completed. Future work will address these gaps and will include direct comparison with previously proposed STS models. Additionally, electromyography (EMG) recordings may be incorporated to relate predicted torque patterns to underlying neuromuscular activity, providing an independent basis for validating and refining model predictions.

Author Contributions: Conceptualization, A.A.; methodology, A.A.; software, A.A. and S.G.; validation, A.A. and S.G.; formal analysis, A.A. and S.G.; investigation, A.A. and S.G.; writing—original draft preparation, A.A. and S.G.; writing—review and editing, A.A., S.G. and R.Z.; visualization, A.A. and S.G.; supervision, A.A. and R.Z. All authors have read and agreed to the published version of the manuscript.

Funding: This research received no external funding.

Institutional Review Board Statement: Not applicable.

Informed Consent Statement: Not applicable.

Data Availability Statement: The original contributions presented in this study are included in the article, the M-files used to generate the figures can be accessed via https://github.com/amery1967/STS_Optimization.git (accessed on 6 February 2026). Further inquiries can be directed to the corresponding author.

Acknowledgments: We acknowledge the support of Sultan Qaboos University in facilitating the resources needed to run the simulations.

Conflicts of Interest: The authors declare no conflicts of interest.

Abbreviations

The following abbreviations are used in this manuscript:

STS	Sit-To-Stand
HAT	Head–arms–trunk
DOFs	Degrees of freedom
COG	Centre of gravity
GRF	Ground reaction force
STW	Sit-to-walk
Parameters and Greek symbols:	
I	Moment of inertia
g	Gravity constant
$\mathcal{L}$	Lagrangian
R	Raleigh dissipation function
v_{Gi}	Velocity of the centre of gravity of i
y_{Gi}	Centre of gravity of i
m_i	Mass of i
k_i	Spring constant
c_i	Damping coefficient
θ	Angular displacement
$\mathcal{L}_d$	Discrete Lagrange
$D_1\mathcal{L}_d$	Frist derivative of $\mathcal{L}_d$ w.r.t. current coordinates
$D_2\mathcal{L}_d$	Frist derivative of $\mathcal{L}_d$ w.r.t. future coordinates
f_d	Discrete forces (torques at joints)
J	Cost function

References

1. Van Der Kruk, E.; Silverman, A.K.; Reilly, P.; Bull, A.M.J. Compensation due to age-related decline in sit-to-stand and sit-to-walk. *J. Biomech.* **2021**, *122*, 110411. [CrossRef]
2. Dall, P.M.; Kerr, A. Frequency of the sit to stand task: An observational study of free-living adults. *Appl. Ergon.* **2010**, *41*, 58–61. [CrossRef]
3. Bohannon, R.W. Five-repetition sit-to-stand test performance by community-dwelling adults: A preliminary investigation of times, determinants, and relationship with self-reported physical performance. *Isokinet. Exerc. Sci.* **2007**, *17*, 77–81. [CrossRef]
4. Gharib, N.M.M.; Rehab, N.I.; Rezk-Allah, S.S. Sagittal lumbar motion during sit-to-stand task and its relation to balance in chronic stroke patients. *Bull. Fac. Phys. Ther.* **2017**, *22*, 59–65. [CrossRef]

5. Abujaber, S.B.; Marmon, A.R.; Pozzi, F.; Rubano, J.J.; Zeni, J.A., Jr. Sit-To-Stand Biomechanics Before and After Total Hip Arthroplasty. *J. Arthroplast.* **2015**, *30*, 2027–2033. [CrossRef] [PubMed]
6. Schenkman, M.; Riley, P.O.; Pieper, C. Sit to stand from progressively lower seat heights—Alterations in angular velocity. *Clin. Biomech.* **1996**, *11*, 153–158. [CrossRef]
7. Bohannon, R.W.; Bubela, D.J.; Magasi, S.R.; Wang, Y.-C.; Gershon, R.C. Sit-to-stand test: Performance and determinants across the age-span. *Isokinet. Exerc. Sci.* **2010**, *18*, 235–240. [CrossRef]
8. Jeon, W.; Whitall, J.; Griffin, L.; Westlake, K.P. Trunk kinematics and muscle activation patterns during stand-to-sit movement and the relationship with postural stability in aging. *Gait Posture* **2021**, *86*, 292–298. [CrossRef]
9. Johnson, M.B.; Cacciatore, T.W.; Hamill, J.; Van Emmerik, R.E. Clinical Biomechanics Multi-segmental torso coordination during the transition from sitting to standing. *Clin. Biomech.* **2010**, *25*, 199–205. [CrossRef]
10. Pourahmadi, M.R.; Takamjani, I.E.; Jaberzadeh, S.; Sarrafzadeh, J.; Sanjari, M.A.; Bagheri, R.; Taghipour, M. Kinematics of the Spine During Sit-to-Stand Movement Using Motion Analysis Systems: A Systematic Review of Literature. *J. Sport Rehabil.* **2019**, *28*, 77–93. [CrossRef]
11. Jeyasurya, J.; Van der Loos, H.F.M.; Hodgson, A.; Croft, E.A. Comparison of seat, waist, and arm sit-to-stand assistance modalities in elderly population. *J. Rehabil. Res. Dev.* **2013**, *50*, 835–844. [CrossRef]
12. Li, J.; Xue, Q.; Yang, S.; Han, X.; Zhang, S.; Li, M.; Guo, J. Kinematic analysis of the human body during sit-to-stand in healthy young adults. *Medicine* **2021**, *100*, e26208. [CrossRef] [PubMed]
13. Ho Hoang, K.-L.; Mombaur, K.D. Optimal design of a physical assistive device to support sit-to-stand motions. In Proceedings of the IEEE International Conference on Robotics and Automation, Seattle, WA, USA, 26–30 May 2015; pp. 5891–5897. [CrossRef]
14. Rea, P.; Ruggiu, M.; Ottaviano, E. Synthesis and Prototyping of a Sit-to-Stand Assisting Device †. *Machines* **2024**, *12*, 33. [CrossRef]
15. Yang, S.; Jia, P.; Zhao, N.; Zhang, S.; Xue, Q. Effect analysis of seat height on sit-to-stand movement stability in healthy young adults. *Int. J. Intell. Robot. Appl.* **2024**, *8*, 1028–1037. [CrossRef]
16. Aissaoui, R.; Dansereau, J. Biomechanical analysis and modelling of sit to stand task: A literature review. In Proceedings of the IEEE International Conference on Systems, Man and Cybernetics, Tokyo, Japan, 12–15 October 1999; pp. 141–146. [CrossRef]
17. Norman-Gerum, V.; McPhee, J. Comprehensive description of sit-to-stand motions using force and angle data. *J. Biomech.* **2020**, *112*, 110046. [CrossRef]
18. Schenkman, M.; A Berger, R.; O Riley, P.; Mann, R.W.; Hodge, W.A. Whole-body movements during rising to standing from sitting. *Phys. Ther.* **1990**, *70*, 638–651. [CrossRef]
19. Janssen, W.G.; Bussmann, H.B.; Stam, H.J. Determinants of the sit-to-stand movement: A review. *Phys. Ther.* **2002**, *82*, 866–879. [CrossRef]
20. An, S.-H.; Park, D.-S. The Effects of Trunk Exercise on Mobility, Balance and Trunk Control of Stroke Patients. *J. Korean Soc. Phys. Med.* **2017**, *12*, 25–33. [CrossRef]
21. Yoshioka, S.; Nagano, A.; Himeno, R.; Fukashiro, S. Computation of the kinematics and the minimum peak joint moments of sit-to-stand movements. *Biomed. Eng. Online* **2007**, *6*, 26. [CrossRef]
22. Norman-Gerum, V.; McPhee, J. Constrained Dynamic Optimization of Sit-to-Stand Motion Driven by Bézier Curves. *J. Biomech. Eng.* **2018**, *140*, 121011. [CrossRef]
23. Domire, Z.J. A Biomechanical Analysis of Maximum Vertical Jumps and Sit-to-Stand. Ph.D. Thesis, The Pennsylvania State University, University Park, PA, USA, 2004.
24. Prinz, R.K. Synthesizing the Sit-to-Stand Movement Using Fuzzy Logic-Based Control and a Simple Biomechanical Model. Master's Thesis, University of Victoria, Victoria, BC, Canada, 2010.
25. Geravand, M.; Korondi, P.Z.; Werner, C.; Hauer, K.; Peer, A. Human sit-to-stand transfer modeling towards intuitive and biologically-inspired robot assistance. *Auton. Robot.* **2016**, *41*, 575–592. [CrossRef]
26. Onishi, H.; Muromaki, T.; Suda, A.; Tyler, N.; Suzuki, T. Basic Design of a Powered Sit-to-stand Chair with Multi-link System. In Proceedings of the 4th International Conference on Design Engineering and Science, ICDES 2017, Aachen, Germany, 17–19 September 2017; pp. 19–21.
27. Mombaur, K. Optimization of sit to stand motions of elderly people for the design and control of physical assistive devices. *PAMM* **2014**, *14*, 805–806. [CrossRef]
28. Yang, J.; Ozsoy, B. Three dimensional unassisted sit-to-stand prediction for virtual healthy young and elderly individuals. *Multibody Syst. Dyn.* **2020**, *49*, 33–52. [CrossRef]
29. Sadeghi, M.; Andani, M.E.; Bahrami, F.; Parnianpour, M. Trajectory of human movement during sit to stand: A new modeling approach based on movement decomposition and multi-phase cost function. *Exp. Brain Res.* **2013**, *229*, 221–234. [CrossRef]
30. Pandy, M.G.; Garner, B.A.; Anderson, F.C. Optimal Control of Non-ballistic Muscular Movements: A constraint-based performance criterion for rising from a chair. *J. Biomech. Eng.* **1995**, *117*, 15–26. [CrossRef]
31. Yokota, H.; Ohshima, S.; Mizuno, N. Sit-to-stand motion analysis using multiobjective genetic algorithm based on musculoskeletal model simulation. *IEEJ J. Ind. Appl.* **2016**, *5*, 236–244. [CrossRef]

32. Mughal, A.M.; Iqbal, K. Sit-to-stand movement with coupled 3D bipedal model for biomechanical torque optimization and experimental analysis. In Proceedings of the 2010 IEEE International Conference on Systems, Man and Cybernetics, Istanbul, Turkey, 10–13 October 2010; pp. 568–573. [CrossRef]
33. Junge, O.; Marsden, J.E.; Ober-Blöbaum, S. Discrete Mechanics and Optimal Control. *IFAC Proc.* **2005**, *38*, 538–543. [CrossRef]
34. Amirouche, F.M.L.; Ider, S.K. Simulation and analysis of a biodynamic human model subjected to low accelerations—A correlation study. *J. Sound Vib.* **1988**, *123*, 281–292. [CrossRef]
35. Gao, K.; Li, C.; Xiao, Y.; Zhang, Z. Finite element modeling and parameter identification of the seated human body exposed to vertical vibration. *Biomech. Model. Mechanobiol.* **2021**, *20*, 1789–1803. [CrossRef]
36. Serbest, K.; Cilli, M.; Eldogan, O. Biomechanical effects of daily physical activities on the lower limb. *Acta Orthop. Traumatol. Turc.* **2015**, *49*, 85–90. [CrossRef]
37. Bajd, T.; Kralj, A.; Turk, R. Standing-up of a healthy subject and a paraplegic patient. *J. Biomech.* **1982**, *15*, 1–10. [CrossRef]
38. Fleckenstein, S.J.; Kirby, R.; MacLeod, D.A. Effect of limited knee-flexion range on peak hip moments of force while transferring from sitting to standing. *J. Biomech.* **1988**, *21*, 915–918. [CrossRef]
39. Pai, Y.-C.; Rogers, M.W. Control of body mass transfer as a function of speed of ascent in sit-to-stand. *Med. Sci. Sports Exerc.* **1990**, *22*, 378–384. [CrossRef]
40. Rodosky, M.W.; Andriacchi, T.P.; Andersson, G.B.J. The Influence of Chair Height on Lower Limb Mechanics During Rising. *J. Orthop. Res.* **1989**, *7*, 266–271. [CrossRef]
41. Pai, Y.-C.; Rogers, M.W. Speed Variation and Resultant During Sit-to-Stand. *Arch Phys. Med. Rehabil.* **1991**, *72*, 881–885. [CrossRef]
42. Kelley, G.; Dainis, D.L.; Wood, A. Mechanics and muscular dynamics of rising from a seated position. *Int. Ser. Biomech. Biomech.* **1976**, *1*, 127–134.
43. Shepherd, R.B.; Gentile, A.M. Sit-to-stand: Functional relationship between upper body and lower limb segments. *Hum. Mov. Sci.* **1994**, *13*, 817–840. [CrossRef]